Materials Advances

ROYAL SOCIETY OF CHEMISTRY

COMMUNICATION

View Article Online
View Journal | View Issue

Cite this: *Mater. Adv.*, 2025, 6, 3460

Received 14th March 2025,
Accepted 15th May 2025

DOI: 10.1039/d5ma00230c

rsc.li/materials-advances

Potassium cation storage and diffusion in SnS, SnS_2, and at SnS/SnS_2 interfaces†

Christoph Kirsch, Daniel Sebastiani and Pouya Partovi-Azar *

Due to their promising performance, tin sulfide and tin disulfide have been investigated as anode materials in various types of batteries, such as Li-, Na-, and K-ion batteries. Understanding the thermodynamics and kinetics of processes involving metal ions at the atomistic level, and how these processes differ between tin sulfide and tin disulfide, is crucial for improving their electrochemical performance in respective applications. However, a direct comparison between these two materials during battery operation has been limited so far. Here, we report on potassium cation diffusion barriers in bulk tin sulfide and tin disulfide, as well as parallel and perpendicular to several SnS/SnS_2 interfaces by means of density functional theory calculations. We also investigate the thermodynamics of potassium storage in these materials. Our results demonstrate that while K^+ diffusion in SnS occurs through elemental processes involving lower energy barriers, potassium storage in SnS_2 is thermodynamically more favorable. These observations suggest strategies to improve the overall electrochemical performance of SnS/SnS_2 heterostructures in battery applications.

1. Introduction

Tin sulfide (SnS) and tin disulfide (SnS_2) have had a wide range of uses, ranging from earlier optoelectronic applications, such as solar cells[1–4] and photodetectors,[5–9] to ongoing investigations into their potential as battery materials. They were first proposed as conversion-type anode materials for lithium-ion batteries (LIBs), due to their high theoretical capacity and layered structure.[10–16] SnS_2 has also been studied as an anode material for sodium-ion batteries (SIBs), particularly due to its increased interlayer spacing, making it more suitable for accommodating larger Na^+ ions.[12,17–19] Both SnS and SnS_2 have recently been studied as electrode materials for potassium-ion batteries (PIBs)[20–26] and lithium–sulfur batteries (LSBs)[27–30] as well. It has been shown that tin-based heterostructures,[31] SnS_2 nanosheets anchored to doped MXene sheets,[32] or composite materials out of SnS_2 and reduced graphene oxide[33,34] or doped carbon nanofibers[21] could exhibit an improve electrochemical performance as anodes for potassium-ion batteries, partially due to metallic nature of the underlying carbonaceous material.[35,36] However, in their battery-related applications, challenges arise due to their volume expansion during battery operation, low electrical conductivity, and sluggish kinetics.[37] SnS/SnS_2 heterostructures have been proposed to provide better structural stability,[6,29,38] while anchoring these heterostructures to reduced graphene oxide is believed to enhance overall electronic conductivity and rate performance.[39–41]

However, poor kinetics of metal ion diffusion in these structures still poses a major challenge, especially in the case of PIBs involving large potassium ions. In order to improve the kinetics of cation intercalation and diffusion, it is necessary to gather an atomistic picture on the underlying fundamental processes. In addition, a deeper comparative understanding of the thermodynamics of metal cation storage in SnS and SnS_2 will help further optimize the morphology of SnS/SnS_2 heterostructure for more efficient batteries. In this communication, we study the potassium cation diffusion in bulk SnS and SnS_2, as well as at SnS/SnS_2 interfaces by means of quantum-chemical calculations. Moreover, the thermodynamics of potassium storage in the bulk materials and the charge distribution at the interface are investigated and discussed.

2. Methodology

We constructed supercells of bulk SnS ($2 \times 4 \times 4$) and SnS_2 ($4 \times 4 \times 4$) from experimental crystallographic data[42,43] (Fig. 1). In this study, VMD[44] is used for visualization of all systems.

Institute of Chemistry, Martin Luther University Halle-Wittenberg, Von-Danckelmann-Platz 4, 06120 Halle (Saale), Germany.
E-mail: pouya.partovi-azar@chemie.uni-halle.de

† Electronic supplementary information (ESI) available. See DOI: https://doi.org/10.1039/d5ma00230c

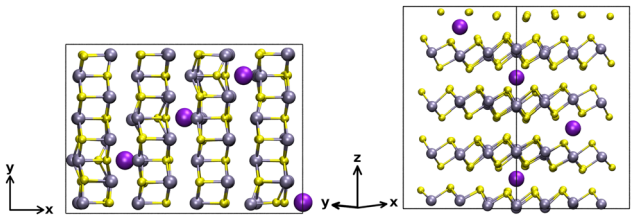

Fig. 1 Structures of bulk SnS (left) and SnS_2 (right) together with potassium ions considered in this work for *ab initio* molecular dynamics and nudged elastic band calculations. Tin atoms, sulfur atoms, and potassium ions are shown in gray, yellow, and purple. The same color coding is used throughout this paper.

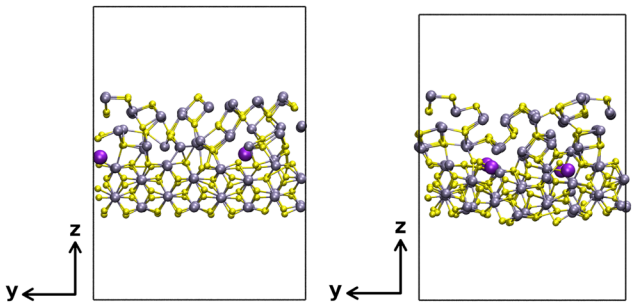

Fig. 2 Two model SnS/SnS_2 interfaces formed by a (302) surface slab of SnS and a (110) surface slab of SnS_2 with two different terminations, labeled as interface 1a (left panel) and interface 1b (right panel).

We further constructed SnS/SnS_2 interfaces using pymatgen[45] from a (302) SnS surface slab and a (110) SnS_2 surface slab with two different terminations, as shown in Fig. 2.

Finally, a SnS/SnS_2 interface was constructed from a (020) surface slab of SnS and a (110) surface slab of SnS_2 (Fig. 3).

The lattice constants and atomic coordinates of all structures were fully relaxed; the resulting configurations are shown in the ESI.† Subsequently, four K^+ ions were added to each system, followed by a second relaxation step. Atomic coordinates of the relaxed systems are given as ESI.†[46] The resulting structures were used in density functional theory (DFT)-based *ab initio* molecular dynamics (AIMD) simulations to identify possible diffusion paths in each system.

DFT[47,48] calculations were performed using the CP2K[49,50]/QUICKSTEP[50–52] software together with a DZVP-MOLOPT-SR-GTH basis set[53] for the valence electrons, and Goedecker–Teter–Hutter (GTH) pseudopotentials.[54–56] To account for exchange and correlation (XC) effects, we applied the Perdew–Burke–Ernzerhof (PBE) functional,[57,58] together with the semi-empirical DFT-D3 method[59] with Becke–Johnson (BJ) damping[60] and revised damping parameters[61] to correct for the long-range dispersion interactions. A plane-wave energy cutoff of 350 Ry and a relative cutoff of 40 Ry were chosen. Only the Γ point was considered due to the large supercells and the convergence criterion for self-consistent field cycles was set to 10^{-6}. Periodic boundary conditions were used for all calculations.

AIMD simulations were carried out in a canonical ensemble (NVT) at 500 K for 40 ps to 100 ps using a Nosé–Hoover chain thermostat.[62,63] A time step of 2 fs was chosen for atomic coordinate propagation.

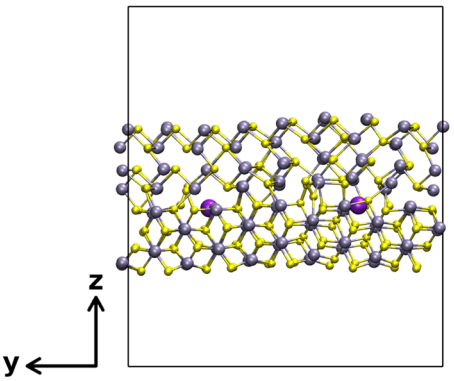

Fig. 3 A model SnS/SnS_2 interface formed by a (020) surface slab of SnS and a (110) surface slab of SnS_2, labeled as interface 2.

To calculate the migration barriers for each of the paths obtained through AIMD simulations, climbing image[64] nudged elastic band[65–67] (CI-NEB) calculations were performed. In the CI-NEB calculations, the number of replicas and the spring constant were set to 8 and 2.0×10^{-2} a.u., respectively.

Layer-resolved sums of charges perpendicular to the interface (along *z* axis) were calculated using different approaches, namely density-derived atomic point charges (DDAPC),[68] Hirshfeld,[69] Mulliken,[70] and restrained electrostatic potential (RESP).[71]

3. Results and discussion

Our AIMD simulations at 500 K reveal that, in bulk SnS, K^+ ions migrate *via* low-energy path (1) shown in Fig. 4(a). Moreover, we observe a reversible K ↔ Sn substitution, hindering the diffusion of potassium in the lattice. In bulk SnS_2, however, no K^+ migration is observed. In the AIMD simulations of interfaces 1a and 1b (Fig. 2), no diffusion is detected either. However, we observe K^+ migration at interface 2 *via* paths (7) to (10) [Fig. 4(g)–(j)]. The corresponding K^+ diffusion coefficients computed from the mean square displacements (MSDs) using TRAVIS[72,73] are 81 $pm^2\ ps^{-1}$ and 230 $pm^2\ ps^{-1}$ for bulk SnS and interface 2, respectively.

Altogether, we studied ten migration pathways: path (1) from the AIMD simulation for SnS [Fig. 4(a)], one theoretically constructed path (2) for SnS_2 [Fig. 4(b)], four theoretically constructed paths (3) to (6) for interface 1b [Fig. 4(c)–(f)], and four paths (7) to (10) from the MD simulation for interface 2 [Fig. 4(g)–(j)]. Atomic coordinates of the fully relaxed diffusion paths together with the respective energy profiles are provided as ESI.†[46] Energy barriers are given in Table 1. Note that the asymmetry of migration barriers in SnS and SnS_2 is due to the presence of adjacent K^+ ions. In principle, the initial and final K^+ interstitial sites are crystallographically equivalent within paths (1) and (2).

Path (2) is higher in energy than path (1), showing better K^+ diffusion kinetics in SnS. At high charge/discharge rates, this

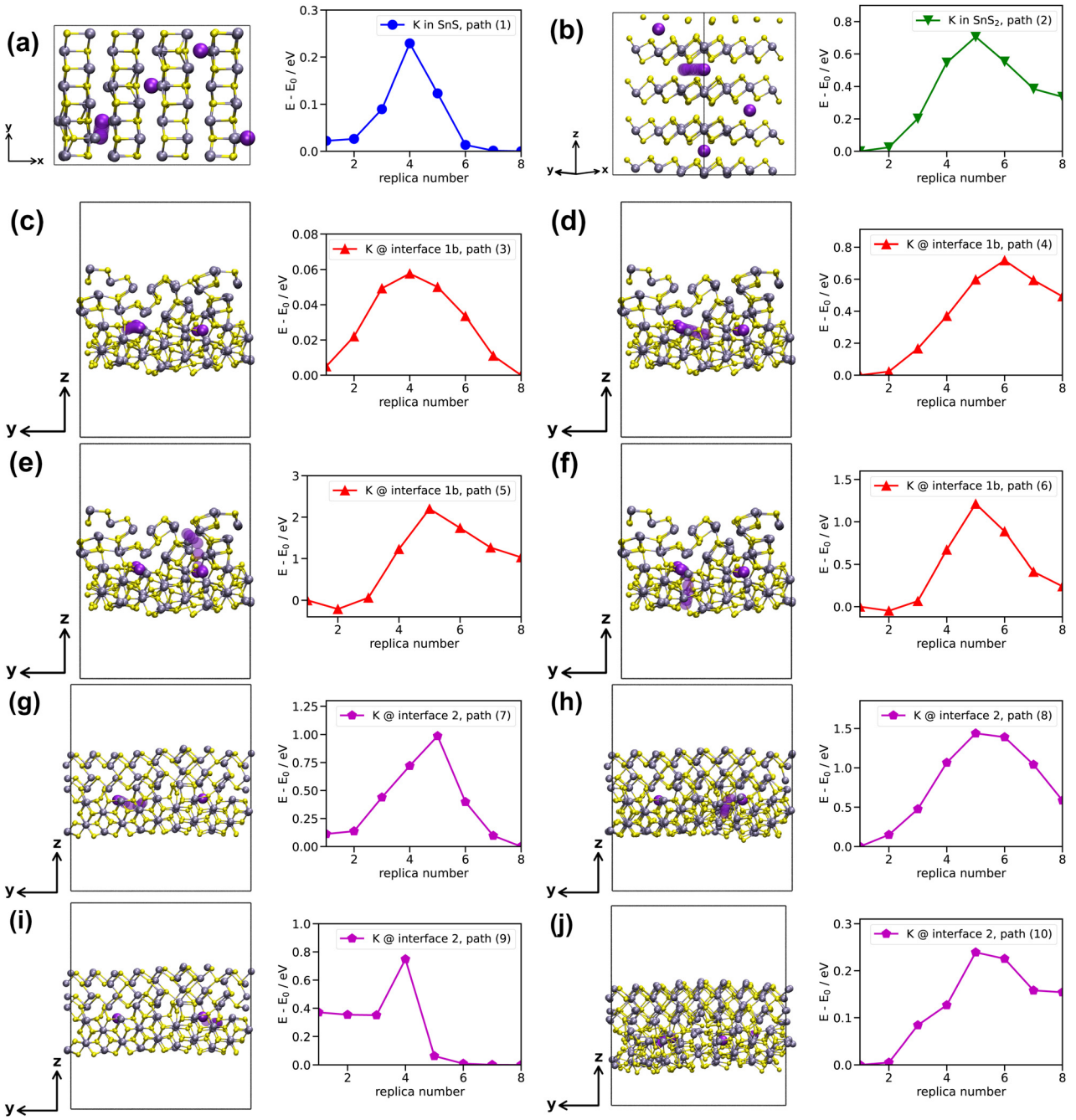

Fig. 4 K^+ migration paths and corresponding energy profiles in different structures: (a) path (1) in bulk SnS; (b) path (2) in bulk SnS_2; (c)–(f) paths (3)–(6) at SnS/SnS_2 interface 1b; (g)–(j) paths (7)–(10) at SnS/SnS_2 interface 2.

could suggest better electrochemical performance of SnS-containing electrodes than of those involving SnS_2, since at a higher current rate the kinetics becomes more important. For Na-ion batteries, this improved rate performance for SnS has been measured.[40] We constructed two paths (3) and (4) parallel to interface 1b [Fig. 4(c) and (d)], as well as two paths (5) and (6) perpendicular to it [Fig. 4(e) and (f)]. K^+ migration parallel to the interface is significantly more facile than perpendicular to it, with energy barriers comparable to bulk SnS and SnS_2. Note that all interfacial paths (3) to (10) alone cannot mediate long-range diffusion. This is particularly true for low-energy path (3), which must be followed by path (4) for effective migration in the *y*-direction. Higher diffusion barriers perpendicular to the interface indicate possibly hindered K^+ motion between the two materials in a heterostructure. For interface 2, paths (7), (9) and (10) describe migration parallel to the interface and path (8) perpendicular to it. Paths (7) and (8) have rather high barriers, while paths (9) and (10) are again comparable to the bulk materials.

Overall, we conclude that K^+ diffusion kinetics in bulk SnS is faster than in bulk SnS_2, suggesting that a heterostructure

Table 1 K^+ migration barriers ΔE^M in SnS, SnS_2 and at SnS/SnS_2 interfaces for the forward (→) and backward (←) processes, along with jump distances d

System	Path no.	d/Å	$\Delta E^M_{\rightarrow}$/eV	$\Delta E^M_{\leftarrow}$/eV
Bulk SnS	(1)	1.76	0.21	0.23
Bulk SnS_2	(2)	3.31	0.71	0.37
Interface 1b	(3)	1.88	0.05	0.06
	(4)	3.89	0.72	0.23
	(5)	6.17	2.42	1.17
	(6)	5.21	1.26	0.97
Interface 2	(7)	4.28	0.87	0.99
	(8)	3.86	1.44	0.85
	(9)	2.30	0.38	0.75
	(10)	2.51	0.24	0.09

could benefit from more facile diffusion in SnS. In addition, migration parallel to SnS/SnS_2 interfaces shows energy barriers that range between SnS and SnS_2, neither affecting material performance positively nor negatively. Perpendicular to these interfaces, K^+ diffusion is slowest, indicating that an optimal particle size and morphology must be experimentally determined for good anode kinetics. The SnS_2 particles should be small enough to prevent long-range bulk diffusion, while the bulk-to-interface ratio should be large enough to minimize excessive migration across the interfaces.

To study the thermodynamics of potassium intercalation, we calculated the enthalpy of the intercalation reactions as

$$\Delta H^c_{SnS_x} = E(SnS_x/K^c) - E(SnS_x) - E(K^c), \qquad (1)$$

where $x = 1, 2$ and c denotes the reaction involving a potassium atom ($c = 0$) or a cation ($c = +1$). In the calculation of enthalpies, volume expansion was assumed to have a negligible contribution. The difference between the K^+ intercalation enthalpies in SnS and SnS_2, defined as $\Delta\Delta H^{+1} = \Delta H_{SnS_2}{}^{+1} - \Delta H_{SnS}{}^{+1}$, was obtained to be around −1.335 eV, while $\Delta\Delta H^0 \simeq -1.762$ eV in the case of a neutral potassium atom. This clearly shows a more thermodynamically favorable potassium storage in bulk SnS_2, resulting in a lower potential difference to the cathode material. Moreover, the theoretical capacities of SnS and SnS_2 for potassium storage, as reported in the literature, are 1136 mA h g^{-1} and 733 mA h g^{-1}, respectively.[25] However, under experimental conditions, the specific capacities and cycling performances in the case of sodium storage are significantly closer.[38,40]

Furthermore, we calculated the sum of charges per layer perpendicular to interface 1b using different theoretical approaches (Fig. 5). The layer thickness was set to 2.5 Å. Apart from discrepancies in values obtained *via* different methods, the formation of an interfacial electric field is predicted by all theoretical approaches. This built-in electric field could explain the comparatively higher diffusion barrier from the interface region into the SnS slab [path (5)] compared to the SnS_2 slab [paths (6) and (8)] through electrostatic repulsion and attraction, respectively.

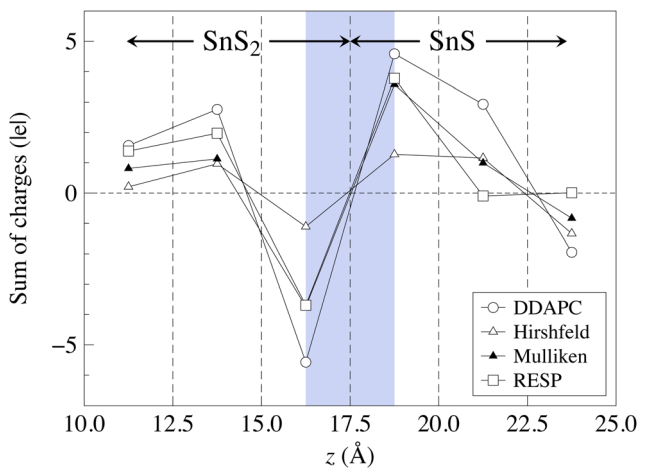

Fig. 5 Layer-wise sum of charges perpendicular to the SnS/SnS_2 interface 1b calculated using different methods. The shaded region highlights the interface.

4. Conclusions

In this study, we report the thermodynamics of potassium storage and the kinetics of K^+ migration in bulk SnS and SnS_2, as well as parallel and perpendicular to different SnS/SnS_2 interfaces, obtained through density functional theory calculations. Our findings reveal that bulk SnS_2 offers thermodynamically more stable potassium storage, while K^+ diffusion is faster in bulk SnS due to atomistic processes with comparatively lower barriers. Therefore, at higher current rates, SnS is expected to outperform SnS_2. These results also suggest potential routes for designing SnS/SnS_2 heterostructures to improve overall battery performance. Diffusion barriers parallel to the SnS/SnS_2 interfaces in the heterostructure are comparable to those in the individual bulk materials. However, our findings show that, despite the formation of an interfacial electric field, K^+ diffusion perpendicular to the interface is the slowest process in SnS/SnS_2 heterostructures overall. Therefore, we propose an experimental optimization of the SnS/SnS_2 heterostructures with respect to bulk-to-interface ratio. In terms of composition, increasing the SnS content leads to better rate performance, while SnS_2 should result in intercalation of potassium starting at lower voltages during the charging process. Our theoretical results hint at synthesis strategies to form SnS/SnS_2 heterostructures that maximize the bulk-to-interface ratio to minimize excessive migration across the interfaces between the two materials.

Author contributions

C. K. contributed to formal analysis, investigation, methodology, visualization, and writing (original draft, review & editing); D. S. contributed to supervision and validation; P. P.-A. contributed to conceptualization, funding acquisition, methodology, supervision, validation, and writing (review & editing).

Data availability

Data supporting this article have been included as part of the ESI.† Data for this article, including relaxed atomic coordinates

of the studied systems and diffusion paths (.xyz files), as well as energy profiles for the latter (.txt files) are available at Zenodo at **https://doi.org/10.5281/zenodo.15011135**.

Conflicts of interest

There are no conflicts to declare.

Acknowledgements

P. P.-A. gratefully acknowledges DFG funding *via* projects 420536636 and 446879138, as well as the computing time made available on the high-performance computer at the NHR Center of TU Dresden *via* the project 'p_oligothiophenes.' The authors also thank Wenxi Wang and Yan Lu for fruitful discussions.

References

1 N. Spalatu, J. Hiie, R. Kaupmees, O. Volobujeva, J. Krustok, I. Oja Acik and M. Krunks, Postdeposition processing of SnS thin films and solar cells: prospective strategy to obtain large, sintered, and doped SnS grains by recrystallization in the presence of a metal halide flux, *ACS Appl. Mater. Interfaces*, 2019, **11**, 17539–17554.

2 J. Y. Cho, S. Kim, R. Nandi, J. Jang, H.-S. Yun, E. Enkhbayar, J. H. Kim, D.-K. Lee, C.-H. Chung and J. Kim, *et al.*, Achieving over 4% efficiency for SnS/CdS thinfilm solar cells by improving the heterojunction interface quality, *J. Mater. Chem. A*, 2020, **8**, 20658–20665.

3 Y. Rui, T. Li, B. Li, Y. Wang and P. Muller-Buschbaum, Two-dimensional SnS_2 nanosheets as electron transport and interfacial layers enable efficient perovskite solar cells, *J. Mater. Chem. C*, 2022, **10**, 12392–12401.

4 M. Li, S. Guo, X. Zhao, S. Quan, X. Wang, M. Wu, R. Liu and D. Weller, Modeling and Simulation of $MAPbI_3$-Based solar cells with SnS_2 as the Electron Transport Layer (ETL) and MoS_2 as the Hole Transport Layer (HTL), *ACS Appl. Electron. Mater.*, 2024, **6**, 5997–6004.

5 L. Shooshtari, A. Esfandiar, Y. Orooji, M. Samadpour and R. Rahighi, Ultrafast and stable planar photodetector based on SnS_2 nanosheets/perovskite structure, *Sci. Rep.*, 2021, **11**, 19353.

6 S. Veeralingam and S. Badhulika, Coaxial SnS_2/SnS nanostructures on the Ag fiber substrate for flexible self-powered photodetectors, *ACS Appl. Nano Mater.*, 2023, **6**, 3863–3872.

7 M. Kumar, B.-R. Huang, A. Saravanan, H. Sun and S.-C. Chen, Self-Powered Broadband Photodetectors Based on Si/SnS_2 and Si/$SnSe_2$ p–n Heterostructures, *Adv. Electron. Mater.*, 2024, **10**, 2400164.

8 D.-H. Shin, J. Yang, S. Mukherjee, A. Bahrami, S. Lehmann, N. Nasiri, F. Krahl, C. Pang, A. Wrzesínska-Lashkova and Y. Vaynzof, *et al.*, SnS_2 Thin Film with In Situ and Controllable Sb Doping via Atomic Layer Deposition for Optoelectronic Applications, *Adv. Mater. Technol.*, 2024, **9**, 2302049.

9 A. K. Tolloczko, J. Ziembicki, M. Grodzicki, J. Serafínczuk, M. Rosmus, N. Olszowska, S. Gorantla, M. Erdi, S. A. Tongay and R. Kudrawiec, Linear dichroism of the optical properties of SnS and SnSe van der Waals crystals, *Small*, 2025, 2410903.

10 T.-J. Kim, C. Kim, D. Son, M. Choi and B. Park, Novel SnS_2-nanosheet anodes for lithium-ion batteries, *J. Power Sources*, 2007, **167**, 529–535.

11 Z. Liu, H. Deng and P. P. Mukherjee, Evaluating pristine and modified SnS_2 as a lithiumion battery anode: a first-principles study, *ACS Appl. Mater. Interfaces*, 2015, **7**, 4000–4009.

12 Y. Xie, M. Fan, T. Shen, Q. Liu and Y. Chen, SnS_2 nanoplates as stable anodes for sodium ion and lithium ion batteries, *Mater. Technol.*, 2016, **31**, 646–652.

13 Z. X. Huang, Y. Wang, B. Liu, D. Kong, J. Zhang, T. Chen and H. Y. Yang, Unlocking the potential of SnS_2: Transition metal catalyzed utilization of reversible conversion and alloying reactions, *Sci. Rep.*, 2017, **7**, 41015.

14 Q. Pan, F. Zheng, Y. Wu, X. Ou, C. Yang, X. Xiong and M. Liu, MoS_2-covered SnS nanosheets as anode material for lithium-ion batteries with high capacity and long cycle life, *J. Mater. Chem. A*, 2018, **6**, 592–598.

15 J. Mei, J. Han, F. Wu, Q. Pan, F. Zheng, J. Jiang, Y. Huang, H. Wang, K. Liu and Q. Li, SnS@C nanoparticles anchored on graphene oxide as high-performance anode materials for lithium-ion batteries, *Front. Chem.*, 2023, **10**, 1105997.

16 M. Pang, Z. Song, S. Jiang, R. Zhang, Y. Xi, Z. Wu, Y. Jiao and J. Zhao, Carboncoated SnS/NiS heterostructures scattered on the rGO lamellas as composite anode for lithium-ion batteries, *J. Alloys Compd.*, 2025, **1010**, 177272.

17 S. Li, Z. Zhao, C. Li, Z. Liu and D. Li, SnS_2@C hollow nanospheres with robust structural stability as high-performance anodes for sodium ion batteries, *Nano-Micro Lett.*, 2019, **11**, 1–9.

18 G. Chen, X. Yao, Q. Cao, S. Ding, J. He and S. Wang, Flexible free-standing SnS_2/carbon nanofibers anode for high performance sodium-ion batteries, *Mater. Lett.*, 2019, **234**, 121–124.

19 Y. Sun, Y. Yang, X.-L. Shi, G. Suo, H. Chen, M. Noman, X. Tao and Z.-G. Chen, Hierarchical SnS_2/carbon nanotube@reduced graphene oxide composite as an anode for ultra-stable sodium-ion batteries, *Chem. Eng. J. Adv.*, 2020, **4**, 100053.

20 L. Wu, H. Shao, C. Yang, X. Feng, L. Han, Y. Zhou, W. Du, X. Sun, Z. Xu and X. Zhang, *et al.*, SnS_2 nanosheets with RGO modification as high-performance anode materials for Na-ion and K-ion batteries, *Nanomaterials*, 2021, **11**, 1932.

21 D. Li, L. Dai, X. Ren, F. Ji, Q. Sun, Y. Zhang and L. Ci, Foldable potassium-ion batteries enabled by free-standing and flexible SnS_2@C nanofibers, *Energy Environ. Sci.*, 2021, **14**, 424–436.

22 C. Li, Y. An, L. Wang, K. Wang, X. Sun, F. Su, X. Zhang and Y. Ma, Elucidating the Potassiation Mechanism in SnS_2 from a First-Principles Perspective, *J. Phys. Chem. C*, 2023, **127**, 18809–18820.

23 J. Zhang, S. Chen, Z. Huang, W. Zhang, Z. Yuan, Y. Liu, W. Mai and J. Li, Exploring the electrochemical stability

mechanism of a SnS_2-based composite in dimethoxyethane electrolytes for potassium ion batteries, *New J. Chem.*, 2023, **47**, 1979–1984.

24 Q. Peng, J. Rehman, M. K. Butt, S. A. Shafiee, Z. Yang, M. Ouladsmane, J. Liu, M. Ullah and Z. Li, Two-Dimensional SnS and SnSe as Hosts of K-Ion Storage: a First-Principles Prediction, *J. Phys. Chem. C*, 2023, **127**, 15730–15737.

25 A. P. Nowak, A. Rokicínska, Z. Wang, M. Przesniak-Welenc, Z. Zarach, K. Tao, D. Roda, M. Szkoda, K. Trzcínski and J. Li, *et al.*, Experimental and computational analysis of SnSx encapsulated into carbonized chitosan as electrode material for potassium ion batteries, *Sci. Rep.*, 2024, **14**, 31212.

26 C. Li, H. Yu, P. Dong, D. Wang, X. Zeng, J. Wang, Z. Zhang, Y. Zhang, A. Sarapulova and X. Luo, *et al.*, Constructing Hollow Microcubes SnS_2 as Negative Electrode for Sodium-ion and Potassium-ion Batteries, *Chem. – Eur. J.*, 2024, **30**, e202304296.

27 L. Luo, S.-H. Chung and A. Manthiram, A three-dimensional self-assembled SnS_2-nanodots@ graphene hybrid aerogel as an efficient polysulfide reservoir for high-performance lithium–sulfur batteries, *J. Mater. Chem. A*, 2018, **6**, 7659–7667.

28 M. Wang, L. Fan, X. Wu, Y. Qiu, Y. Wang, N. Zhang and K. Sun, SnS_2/SnO_2 heterostructures towards enhanced electrochemical performance of lithium–sulfur batteries, *Chem. – Eur. J.*, 2019, **25**, 5416–5421.

29 Y. Ma, F. Li, H. Ji, H. Wu, B. Wang, Y. Ren, J. Cao, X. Cao, F. Ding and J. Lu, *et al.*, SnS/SnS_2 Heterostructures Embedded in Hierarchical Porous Carbon as Polysulfides Immobilizer for High-Performance Lithium–Sulfur Batteries, *Langmuir*, 2024, **40**, 5527–5534.

30 H. Liu, R. Li, T. Yang and J. Wang, Construction of SnS_2-modified multi-hole carbon nanofibers with sulfur encapsulated as free-standing cathode electrode for lithium sulfur battery, *Nanotechnology*, 2024, **35**, 215402.

31 Y. Feng, Y. Lv, H. Fu, M. Parekh, A. M. Rao, H. Wang, X. Tai, X. Yi, Y. Lin and J. Zhou, *et al.*, Co-activation for enhanced K-ion storage in battery anodes, *Natl. Sci. Rev.*, 2023, **10**, nwad118.

32 Y. Cao, H. Chen, Y. Shen, M. Chen, Y. Zhang, L. Zhang, Q. Wang, S. Guo and H. Yang, SnS_2 nanosheets anchored on nitrogen and sulfur co-doped MXene sheets for high-performance potassium-ion batteries, *ACS Appl. Mater. Interfaces*, 2021, **13**, 17668–17676.

33 D. Li, Q. Sun, Y. Zhang, L. Chen, Z. Wang, Z. Liang, P. Si and L. Ci, Surface-confined SnS_2@ C@ rGO as high-performance anode materials for sodium-and potassium-ion batteries, *ChemSusChem*, 2019, **12**, 2689–2700.

34 C. Li, K. Pfeifer, X. Luo, G. Melinte, J. Wang, Z. Zhang, Y. Zhang, P. Dong, A. Sarapulova and H. Ehrenberg, *et al.*, Investigation of SnS_2-rGO Sandwich Structures as Negative Electrode for Sodium-Ion and Potassium-Ion Batteries, *ChemSusChem*, 2023, **16**, e202202281.

35 P. Partovi-Azar, S. Panahian Jand and P. Kaghazchi, Electronic, magnetic, and transport properties of polyacrylonitrile-based carbon nanofibers of various widths: densityfunctional theory calculations, *Phys. Rev. Appl.*, 2018, **9**, 014012.

36 P. Partovi-Azar, Sulfur/Polyacrylonitrile-Based N-Terminated Graphene Nanoribbon Cathodes for Li-S Batteries, *Phys. Rev. Appl.*, 2022, **18**, 044072.

37 A. Glibo, N. Eshraghi, Y. Surace, A. Mautner, H. Flandorfer and D. M. Cupid, Comparative study of electrochemical properties of SnS and SnS_2 as anode materials in lithium-ion batteries, *Electrochim. Acta*, 2023, **441**, 141725.

38 J. Lu, S. Zhao, S. Fan, Q. Lv, J. Li and R. Lv, Hierarchical SnS/SnS_2 heterostructures grown on carbon cloth as binder-free anode for superior sodium-ion storage, *Carbon*, 2019, **148**, 525–531.

39 J. Wang, Z. Zhang and H. Zhao, SnS_2–SnS pn heterojunction bonded on graphene with boosted charge transfer for lithium storage, *Nanoscale*, 2021, **13**, 20481–20487.

40 Q. Li, F. Yu, Y. Cui, J. Wang, Y. Zhao and J. Peng, Multilayer $SnS\text{-}SnS_2$@GO heterostructures nanosheet as anode material for Sodium ion battery with high capacity and stability, *J. Alloys Compd.*, 2023, **937**, 168392.

41 S. Zhou, J. Lan, K. Song, Z. Zhang, J. Shi and W. Chen, SnS/SnS_2/rGO heterostructure with fast kinetics enables compact sodium ion storage, *FlatChem*, 2021, **28**, 100259.

42 H. Wiedemeier and H. G. von Schnering, Refinement of the structures of GeS, GeSe, SnS and SnSe. Z, *Kristallogr. Cryst. Mater.*, 1978, **148**, 295–304.

43 M. Ø. Filsø, E. Eikeland, J. Zhang, S. R. Madsen and B. B. Iversen, Atomic and electronic structure transformations in SnS_2 at high pressures: a joint single crystal X-ray diffraction and DFT study, *Dalton Trans.*, 2016, **45**, 3798–3805.

44 W. Humphrey, A. Dalke and K. Schulten, VMD: Visual molecular dynamics, *J. Mol. Graph*, 1996, **14**, 33–38.

45 S. P. Ong, W. D. Richards, A. Jain, G. Hautier, M. Kocher, S. Cholia, D. Gunter, V. L. Chevrier, K. A. Persson and G. Ceder, Python Materials Genomics (pymatgen): A robust, open-source python library for materials analysis, *Comput. Mater. Sci.*, 2013, **68**, 314–319.

46 C. Kirsch, D. Sebastiani and P. Partovi-Azar, Supplementary data for ''Potassium cation storage and diffusion in SnS, SnS_2, and at SnS/SnS_2 interfaces'', *Zenodo*, 2025, DOI: **10.5281/zenodo.15011135**.

47 P. Hohenberg and W. Kohn, Inhomogeneous Electron Gas, *Phys. Rev.*, 1964, **136**, B864–B871.

48 W. Kohn and L. J. Sham, Self-Consistent Equations Including Exchange and Correlation Effects, *Phys. Rev.*, 1965, **140**, A1133–A1138.

49 J. Hutter, M. Iannuzzi, F. Schiffmann and J. VandeVondele, cp2k: atomistic simulations of condensed matter systems, *Wiley Interdiscip. Rev.: Comput. Mol. Sci.*, 2014, **4**, 15–25.

50 T. D. Kuhne, *et al.*, CP2K: An electronic structure and molecular dynamics software package - Quickstep: Efficient and accurate electronic structure calculations, *J. Chem. Phys.*, 2020, **152**, 194103.

51 G. Lippert, J. Hutter and M. Parrinello, A hybrid Gaussian and plane wave density functional scheme, *Mol. Phys.*, 1997, **92**, 477–488.

52 J. VandeVondele, M. Krack, F. Mohamed, M. Parrinello, T. Chassaing and J. Hutter, Quickstep: Fast and accurate density functional calculations using a mixed Gaussian and

plane waves approach, *Comput. Phys. Commun.*, 2005, **167**, 103–128.
53 J. VandeVondele and J. Hutter, Gaussian basis sets for accurate calculations on molecular systems in gas and condensed phases, *J. Chem. Phys.*, 2007, **127**, 114105.
54 S. Goedecker, M. Teter and J. Hutter, Separable dual-space Gaussian pseudopotentials, *Phys. Rev. B*, 1996, **54**, 1703–1710.
55 C. Hartwigsen, S. Goedecker and J. Hutter, Relativistic separable dual-space Gaussian pseudopotentials from H to Rn, *Phys. Rev. B*, 1998, **58**, 3641–3662.
56 M. Krack, Pseudopotentials for H to Kr optimized for gradient-corrected exchangecorrelation functionals, *Theor. Chem. Acc.*, 2005, **114**, 145–152.
57 J. P. Perdew, K. Burke and M. Ernzerhof, Generalized Gradient Approximation Made Simple, *Phys. Rev. Lett.*, 1996, **77**, 3865–3868.
58 J. P. Perdew, K. Burke and M. Ernzerhof, Generalized Gradient Approximation Made Simple, *Phys. Rev. Lett.*, 1996, **77**, 3865 (*Phys. Rev. Lett.*, 1997, **78**, 1396).
59 S. Grimme, J. Antony, S. Ehrlich and H. Krieg, A consistent and accurate ab initio parametrization of density functional dispersion correction (DFT-D) for the 94 elements H-Pu, *J. Chem. Phys.*, 2010, **132**, 154104.
60 S. Grimme, S. Ehrlich and L. Goerigk, Effect of the damping function in dispersion corrected density functional theory, *J. Comput. Chem.*, 2011, **32**, 1456–1465.
61 D. G. A. Smith, L. A. Burns, K. Patkowski and C. D. Sherrill, Revised Damping Parameters for the D3 Dispersion Correction to Density Functional Theory, *J. Phys. Chem. Lett.*, 2016, **7**, 2197–2203.
62 S. Nośe, A molecular dynamics method for simulations in the canonical ensemble, *Mol. Phys.*, 1984, **52**, 255–268.
63 S. Nośe, A unified formulation of the constant temperature molecular dynamics methods, *J. Chem. Phys.*, 1984, **81**, 511–519.
64 G. Henkelman, B. P. Uberuaga and H. Jonsson, A climbing image nudged elastic band method for finding saddle points and minimum energy paths, *J. Chem. Phys.*, 2000, **113**, 9901–9904.
65 G. Mills and H. Jonsson, Quantum and thermal effects in H2 dissociative adsorption: Evaluation of free energy barriers in multidimensional quantum systems, *Phys. Rev. Lett.*, 1994, **72**, 1124–1127.
66 G. Mills, H. Jonsson and G. K. Schenter, Reversible work transition state theory: application to dissociative adsorption of hydrogen, *Surf. Sci.*, 1995, **324**, 305–337.
67 G. Henkelman and H. Jonsson, Improved tangent estimate in the nudged elastic band method for finding minimum energy paths and saddle points, *J. Chem. Phys.*, 2000, **113**, 9978–9985.
68 P. E. Blochl, Electrostatic decoupling of periodic images of plane-wave-expanded densities and derived atomic point charges, *J. Chem. Phys.*, 1995, **103**, 7422–7428.
69 F. L. Hirshfeld, Bonded-atom fragments for describing molecular charge densities, *Theoret. Chim. Acta*, 1977, **44**, 129–138.
70 R. S. Mulliken, Electronic Population Analysis on LCAO–MO Molecular Wave Functions, *J. Chem. Phys.*, 1955, **23**, 1833–1840.
71 D. Golze, J. Hutter and M. Iannuzzi, Wetting of water on hexagonal boron nitride@ Rh(111): a QM/MM model based on atomic charges derived for nano-structured substrates, *Phys. Chem. Chem. Phys.*, 2015, **17**, 14307–14316.
72 M. Brehm and B. Kirchner, TRAVIS – A Free Analyzer and Visualizer for Monte Carlo and Molecular Dynamics Trajectories, *J. Chem. Inf. Model.*, 2011, **51**, 2007–2023.
73 M. Brehm, M. Thomas, S. Gehrke and B. Kirchner, TRAVIS—A free analyzer for trajectories from molecular simulation, *J. Chem. Phys.*, 2020, **152**, 164105.